Targeted Ephemeris Decorrelation Parameter Inflation for Improved LAAS Availability during Severe Ionosphere Anomalies

Shankararaman Ramakrishnan, Jiyun Lee, Sam Pullen, and Per Enge
Stanford University

BIOGRAPHY

Shankararaman Ramakrishnan received the B.E. (Hons.) degree in Electrical and Electronics Engineering from the Birla Institute of Technology and Science – Pilani, India in 2006. He is currently a M.S. candidate at Stanford University in the Department of Aeronautics and Astronautics and is also a member of the Global Positioning System laboratory at Stanford University. His research interests include the Local Area Augmentation System and FPGA-based dual-frequency receiver design.

Jiyun Lee is a Senior GPS Systems Engineer at SiRF Technology, Inc. She received the B.S. degree from Yonsei University, Korea and the M.S. degree in Aerospace Engineering and Science from the University of Colorado at Boulder. She joined the Stanford GPS laboratory in 2000, received her Ph.D. degree from the Aeronautics and Astronautics department in 2005, and continued working as a Post-Doctoral researcher in the GPS laboratory. Her Ph.D. thesis work focused on the development of GPS-based aircraft landing system.

Sam Pullen is a Senior Research Engineer at Stanford University, where he is the director of the Local Area Augmentation System (LAAS) research effort. He has supported the FAA in developing LAAS and WAAS system concepts, requirements, integrity algorithms, and performance models. His current work includes the development of system architectures and algorithms for the next phase of LAAS to support operations up to and including Category III precision landings. He participates in the development of the next generation of GPS, known as "GPS III." Dr. Pullen was awarded the Institute of Navigation (ION) Early Achievement Award in 1999.

Per Enge is a Professor of Aeronautics and Astronautics at Stanford University, where he is the Kleiner-Perkins, Mayfield, Sequoia Capital Professor in the School of Engineering. He is also the Director of the GPS Research Laboratory, which works with the Federal Aviation Administration, U.S. Navy and U.S. Air Force to pioneer systems that augment the Global Positioning System (GPS). Prof. Enge has received the Kepler, Thurlow and Burka Awards from the Institute of Navigation for his work. He is a Member of the National Academy of Engineers (NAE), a Fellow of the ION, and a Fellow of the IEEE.

ABSTRACT

The Local Area Augmentation System (LAAS) is a ground-based differential GNSS system designed to provide precision approach for aircraft landing at a LAAS-equipped airport. While most anomalies affecting the system can be mitigated in the range domain, position-domain geometry screening is essential to mitigate threats from anomalous ionosphere spatial gradients. These can potentially cause large range-domain errors before detection by the LAAS Ground Facility (LGF).

Existing algorithms for position-domain screening inflate the sigma values (σ_{vig} and σ_{pr_gnd}) broadcast by the LAAS Ground Facility (LGF). This ensures that subset satellite geometries (i.e. subsets of a set of approved GPS satellites for which the LGF broadcasts valid corrections) for which unacceptable errors can result are made unavailable to the user. These unsafe subsets are found by comparing the resulting Maximum Ionosphere-Induced Error in Vertical (MIEV) with maximum "safe" navigation system error (NSE) values derived from Obstacle Clearance Surface (OCS) applicable to CAT I precision approaches.

Recent analyses of past ionosphere spatial gradients observed over the Conterminous United States (CONUS) resulted in very high maximum gradients for both low and high-elevation satellites. The new ionosphere anomaly "threat model" for LAAS CAT I specifies a maximum spatial gradient of 375 mm/km for low-elevation satellites (below 15^o) while high-elevation (above 65^o) satellites can experience gradients as high as 425 mm/km. Uniform inflation of the broadcast sigmas for all approved satellites results in a significant drop in system availability under the new threat model.

To minimize this decline, this paper proposes a new algorithm to implement position-domain screening by inflating satellite-specific, targeted ephemeris decorrelation parameters (called "P-values") and σ_{pr_gnd} values. Availability is assessed for ten major airports in the USA. Under normal conditions, 100% availability is achieved for eight airports, while availability for the two remaining airports exceeds 99%. Targeted inflation consistently results in better system availability compared to strategies that inflate all satellites by the same amount, such as the σ_{vig} approach.

INTRODUCTION

The aviation navigation community has been developing, testing and adopting new navigation systems which incorporate the use of the Global Navigation Satellite System (GNSS) for a wide variety of aircraft operations. These include flights over oceanic routes, en route navigation, and in the so-called terminal areas where flights converge in crowded metropolitan airspaces. These systems augment basic ranging signals from GNSS satellites thereby improving the accuracy, availability, integrity and continuity of such systems [7]. Two complementary augmentation systems, known as Space Based Augmentation System and Ground Based Augmentation System, would eventually support the entire gamut of aviation navigation.

The Local Area Augmentation System (LAAS) is an example of a Ground Based Augmentation System developed by the U.S. Federal Aviation Administration. The LAAS Ground Facility (LGF) provides differential corrections to aircraft in the vicinity of a LAAS-equipped airport. The LGF is comprised of multiple reference receivers sited within airport property that are used by the LGF to compute differential corrections. These corrections as broadcast by the LGF on a VHF data link with a signal coverage region of up to 23 n.mi. (45 km) from the LGF at low altitudes [5]. Eventually a LAAS-enabled airport might be able to support Category (CAT) IIIc landings, whose requirements stipulate a Decision Height (DH) of 0-100 ft and a Runway Visual Range (RVR) of less than 1200 ft and also demand guidance along the runway surface. A CAT I LAAS system requires a DH of at least 200 ft and an RVR of at least 2400 ft. Below the DH, the aircraft could be controlled manually by the pilot, who would be able to see the landing runway.

For LAAS to meet its signal-in-space (SIS) integrity requirements, errors in the broadcast pseudorange corrections must be bounded (to the required SIS integrity probability) by the nominal error sigmas broadcast along with the differential pseudorange corrections. Aircraft receiving the LAAS corrections compute Horizontal and Vertical Protection Levels (HPL and VPL) and thereby determine the integrity of any set of satellites visible to the aircraft. While most anomalies which would be potentially hazardous to LAAS can be completely mitigated in the range domain, severe ionosphere anomalies can cause several meters of error in the range domain before being detected by the LGF [9]. Satellite geometries visible to the aircraft are safe to use for CAT-I precision approaches when the VPLs computed are below the safe Vertical Alert Limit (VAL) of 10 meters for that operation. However, because VPL does not account for the possibility of extreme ionosphere spatial gradients, these geometries could be unsafe in the presence of such gradients. Satellite geometry screening in the position domain ensures that any geometry that an aircraft could potentially use is safe even under these extreme ionosphere conditions. The idea of integrity validation directly in the position domain also results in higher system availability compared to achieving the equivalent integrity protection solely in the range domain [11].

LGF position-domain screening algorithms currently compute inflation factors for one or more of the broadcast sigmas (typically, it is $\sigma_{vertical\_iono\_gradient}$, also known as σ_{vig}, that is inflated) such that the resulting errors under anomalous conditions are bounded by a "total navigation error limit" that is derived from the Obstacle Clearance Surface (OCS). OCS error bounds exist to prevent an approaching aircraft from colliding with obstacles along the approach path or the ground. The total navigation error limit derived from the OCS surface is obtained by treating the worst-case error resulting from extreme ionosphere spatial gradients as occurring with a probability of 1.0. Other errors affecting the aircraft flight path, such as fault-free Navigation Sensor Error (NSE), flight technical error (FTE), altimeter error, and height loss on possible missed approach are taken at representative 95% (i.e., 2σ) values (see [12]). Figure 1 shows the resulting tolerable error limits for a LAAS CAT-I approach as a function of the aircraft distance from the threshold or decision height that marks the end of the CAT-I phase of the approach.

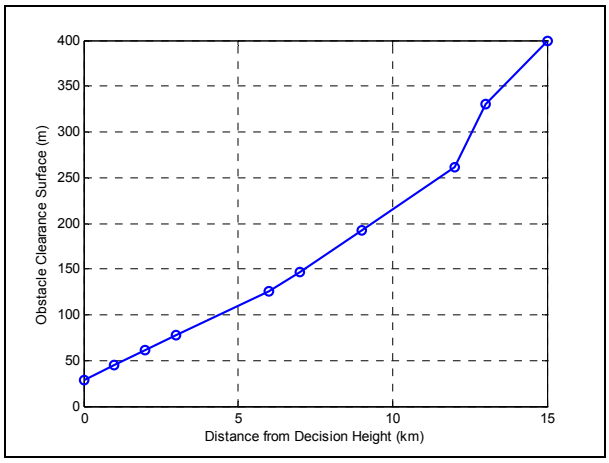

Figure 1: Plot of 95% Tolerable Error Curve for CAT-I LAAS under Worst-Case Ionosphere Anomalies

Figure 2 captures the significance of the tolerable error limit applicable at the threshold point under worst-case ionosphere anomaly conditions. During nominal operating conditions, the VPL must always be below the VAL of 10 meters at the threshold point. However, under the extremely rare circumstance of a worst-case ionosphere anomaly, errors below the tolerable error limit derived from the OCS surface [12] do not pose an unacceptable safety threat to the system. Based on the plot shown in Figure 1, vertical position errors below 28.77 meters at the threshold point are tolerable under the worst-case ionosphere anomaly condition. Errors which exceed this limit must be mitigated by the LGF.

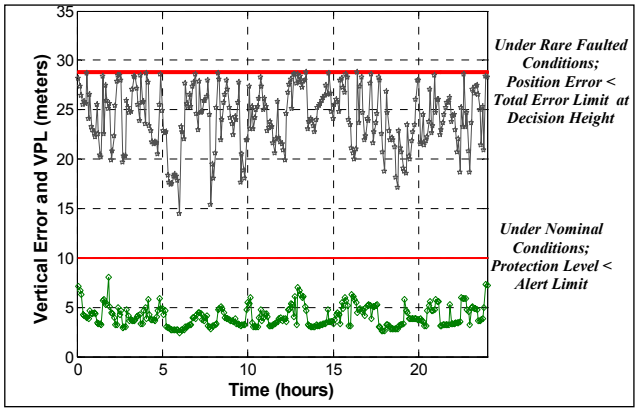

Figure 2: Error Limit Comparison under Nominal and Ionosphere Anomaly Operating Conditions

A recent update to the ionosphere threat model for CONUS resulted in a drop in system availability due to geometry screening using current inflation algorithms [2]. In this paper, we propose a "Targeted Ephemeris Decorrelation Parameter Inflation Algorithm" to more-efficiently determine inflation factors for the broadcast σ_{pr_gnd} and P-values. By "targeted," we mean that inflation factors are determined uniquely for each satellite approved by the LGF. 10 major airports in the Conterminous US were simulated using the proposed algorithm. Simulation results demonstrate that the new algorithm successfully performs position-domain screening to alleviate potential errors which can result from severe ionosphere anomalies while continuing to provide acceptable system availability for the major airports studied.

IONOSPHERE THREAT MODEL

The ionosphere is a dispersive medium extending from a height of 50 km to about 1000 km above the earth's surface and is formed by ionization from solar radiation. Very high temperature in the Sun's upper atmosphere (the corona) causes atoms of hydrogen and helium to escape from the Sun's gravity and transform neutral atoms in the Earth's upper atmosphere into a state of fully ionized plasma [4]. Propagation of radio signals through this plasma region delays the signal by an amount proportional to the Total Electron Content (TEC) of the segment of ionosphere through which the signal passes. While the code phase of GNSS signals is delayed, the carrier phase is advanced by an equal and opposite amount during propagation through the ionosphere. This phenomenon is called "Code-Carrier Divergence".

Under nominal conditions, ionosphere delays on GNSS pseudorange measurements are highly correlated over the short separations between LGF and user ionosphere pierce points (IPP). A conservative one-sigma ionosphere vertical (zenith) gradient value of 4 mm/km proposed to be broadcast by the LGF is sufficient to bound nominal gradients [15]. However analysis of data from past solar storms revealed anomalous ionosphere gradients which were two orders of magnitude larger than those covered by the nominal broadcast sigma values [10]. Such anomalies, if undetected, could result in hazardous user errors.

From the point of view of a user approaching a LAAS-equipped airport, an anomalous ionosphere gradient is modeled as a linear semi-infinite wave front with constant propagation speed, as shown in Figure 3. The gradient is assumed to be a linear change in vertical ionosphere delay between the maximum and minimum delays. The LAAS ionosphere threat model is characterized by three key parameters: the spatial gradient (slope) in slant (not zenith) ionosphere delay, the width of the linear change in delay, and the forward propagation speed (assumed to be constant) of the wave front relative to the ground. Note that the maximum ionosphere delay difference is the product of slope and width and is upper-bounded by a maximum value.

Based on the maximum ionosphere changes observed through analysis of past storm data, slopes and widths whose product results in a maximum delay difference above a pre-defined bound are not part of the threat model. The determination of upper and lower bounds for the parameters of the threat-model, using post-processed WAAS Supertruth data and data from the National Geodetic Survey Continuously Operating Reference Stations (NGS-CORS), is described in [3, 13].

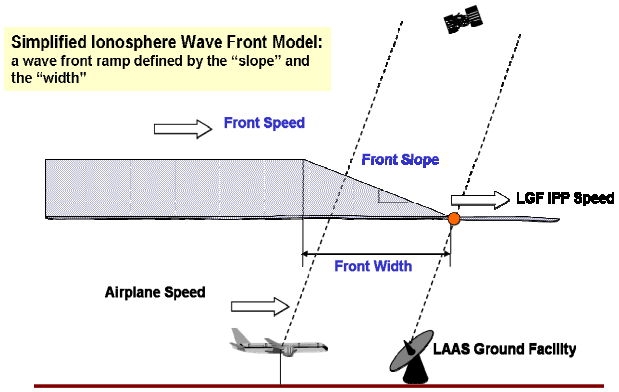

Figure 3: Ionosphere Wave Front Model

Further analysis at Stanford University of data collected from CORS receivers operating in the Ohio/Michigan region during the solar storm of November 20, 2003 revealed upper limits for the ionosphere gradient which were significantly higher than those stated in [1]. Very large gradients were observed for both low and high elevation satellites. Consequently, the ionosphere threat model for LAAS was updated in accord with these new findings.

A. Low Elevation Ionosphere Spatial Anomalies

Using the part-automated, part-manual data analysis procedure described in [1, 3], dual frequency data for satellite (SVN) 26 recorded at CORS stations WOOS and GARF was analyzed. As shown in Figure 4, gradients as high as 360 mm/km were observed for SVN 26 during the period from 20:30 to 21:30 UT. This is significantly larger than the previously validated gradient of 125mm/km for low elevation satellites [1].

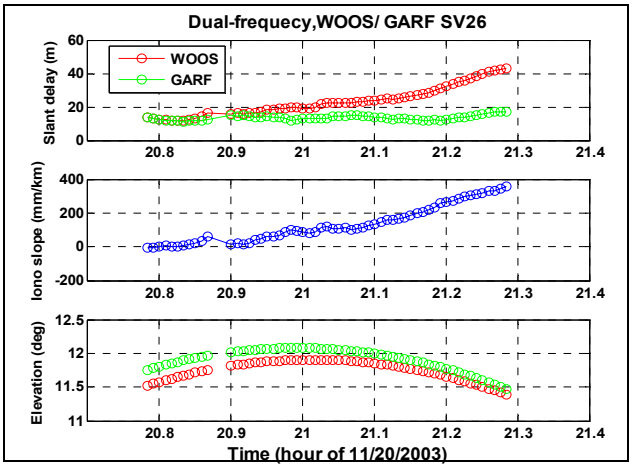

Figure 4: (a) Dual-frequency carrier phase slant measurement of ionosphere delay, in m at L1; (b) Ionosphere spatial gradient versus time; and (c) Elevation of SVN 26 as viewed from WOOS and GARF

B. High Elevation Ionosphere Spatial Anomalies

Significantly larger gradients were observed for high elevation satellites as well. As shown in Figure 5, gradients as high as 412 mm/km were observed between station pairs ZOB1 and GARF while observing SVN 38 during the interval 20:00 to 22:00 UT. This finding was higher then the previous validated maximum gradient of 330 mm/km for high elevation satellites [1].

In line with the findings shown in Figures 4 and 5, and including margin for measurement error, the upper and lower bounds for ionosphere gradients were modified as follows:

i. Low Elevation Satellites (el < 15 degrees) : 375 mm/km

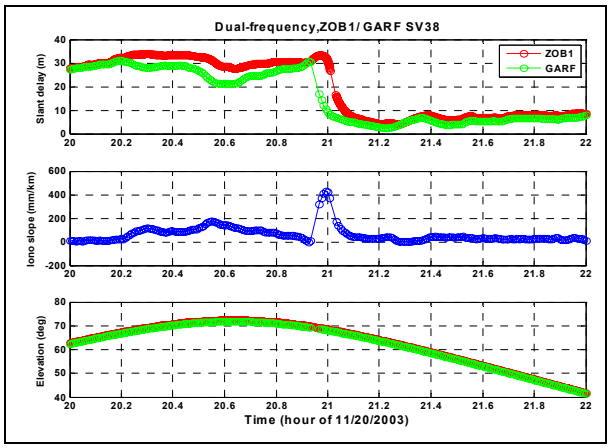

Figure 2: (a) Dual-frequency carrier phase slant measurement of ionosphere delay, in m at L1; (b) Ionosphere spatial gradient; and (c) Elevation of SVN 38 as viewed from ZOB1 and GARF

ii. High Elevation Satellite (el ≥ 65 degrees) : 425 mm/km

iii. Linear interpolation between the upper and lower bounds for satellite elevation in the range [15,65) degrees

A comparison of the slant ionosphere gradient bounds as a function of satellite elevation angle under both old and updated threat models is shown in Figure 6.

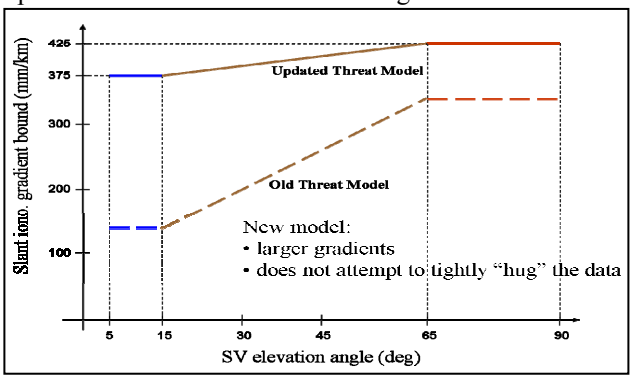

Figure 6: Ionosphere Spatial Gradient as a Function of Satellite Elevation

GBAS RANGE ERRORS DURING IONOSPHERE STORMS

As stated in [1], anomalous ionosphere activity can result in range errors as high as 50 meters. Ionosphere induced range errors (IER) were previously determined using a table look-up methodology as explained in [1, 3]. However in this paper, we present closed-form expressions for determining IER that leverage front velocity as key parameter. The LGF uses a Code-Carrier Divergence (CCD) Monitor to detect anomalous ionospheric activity [16]. The CCD monitor is based on the Code-Carrier Divergence phenomenon explained above. However for

this monitor to detect hazardous spatial gradients, the relative velocity between the LGF IPP velocity projected onto the direction of the front velocity must be reasonably large. For smaller relative velocities, the CCD monitor does not alert, and the undetected user errors can be large. The resulting closed-form range errors can be summarized as follows:

i. Slow Front Speed: 10 m/s < Δv < 40 m/s: There is no CCD detection. The error induced by the ionosphere is proportional to the separation between the LGF and the approaching aircraft. This relationship is expressed as:

$$\varepsilon_1 = \min\left[\frac{50}{W}, G\right] \times (x + 2\tau v_{ac}) \qquad (1)$$

where:

W : Width of the ionosphere front;

G : Gradient of the ionosphere front through which the IPP propagates through;

τ : 100 second smoothing time of the Carrier-Smoothing filter the LGF uses;

v_{ac} : Velocity of the user aircraft during its final approach segment (assumed to be a constant 70 m/s in this paper);

x : Separation between the LGF and the aircraft location.

ii. Moderate Front Speed: 40 m/s < Δv < 110 m/s: For moderate relative velocities between the front and the IPP, the CCD monitor begins to alert (i.e., it alerts for some conditions within this relative-speed range). Consequently, the errors that user aircraft could suffer begin to drop. The maximum range error the aircraft would suffer is no greater the 4 meters.

iii. Fast Front Speed: Δv > 110 m/s: The CCD monitor alerts with a very small missed-detection probability. The maximum range error that users could potentially suffer is no greater than 2.5 meters.

POSITION-DOMAIN GEOMETRY SCREENING

Position-domain geometry screening at the LGF is comprised of two stages:

i. Computing the Maximum Ionosphere Induced Range Error in Vertical (MIEV) for the all-in-view satellite geometry and its associated subsets that an approaching aircraft could potentially use, and

ii. Determining inflation factors for the broadcast sigmas and P-values which would render potentially unsafe geometries unavailable to the aircraft.

These two stages are explained in detail in the subsections that follow.

DETERMINATION OF SUBSET GEOMETRIES

The LGF must ensure that all possible subset geometries obtained from the N satellites approved for use by the LGF are safe to use in combination by an approaching aircraft (in this work, this approved set of N is taken to be the set of satellites visible to the LGF above a 5-degree elevation mask angle). It can be shown that an aircraft during its final approach maneuvering (while inside the precision approach region, or PAR) is very unlikely to simultaneously lose tracking of more than two satellites out of the N approved satellites. Hence, the LGF needs to protect all subsets with two or fewer satellites removed from the N satellites that constitute the approved set. The maximum number of subsets, α, for which the LGF must ensure integrity is given by:

$$\alpha = \sum_{k=N-2}^{N} \binom{N}{k} \qquad (2)$$

Note that (2) is not correct in practice because of the presence of geometries where N exceeds 10 satellites. Because the LAAS MOPS requires that 10-channel receivers be supported [5], geometries where N exceeds 10 create a set of N_{10} independent "sub-approved" geometries with $N' = 10$ satellites each. In this case, all subsets of two or fewer satellites removed from each independent set of N' satellites must also be protected. While each sub-approved set is not identical to any other, satellite removals will make some subsets of a given sub-approved set $N_{10,}^{\ i}$ equivalent to some subsets of another sub-approved set N_{10}^{j}, making it cumbersome to count the total number of subsets to be protected except through actual enumeration (which the LGF must do in real time to determine inflation factors, as described below).

The ionosphere anomaly threat model dictates that no more than two satellites in a given geometry can be simultaneously affected by an anomalous ionosphere front. This is referred to as the two-satellites-impacted scenario. Since the worst possible satellite pair cannot be predicted a-priori, all possible satellite pairs (S_1, S_2) must be considered for each subset geometry. Thus, the total number of pairs, β, for a given approved set with N satellites is computed as:

$$\beta_N = \sum_{k=N-2}^{N} \binom{N}{k}\binom{k}{2} \qquad (3)$$

COMPUTATION OF MAXIMUM IONOSPHERE INDUCED ERROR IN VERTICAL (MIEV)

As outlined in [1], range error computations must consider the impact of both stationary and fast-moving ionosphere fronts for each satellite and two-satellite pair. Range errors in [1] were computed using a range error table lookup procedure. The range errors for each satellite pair in this paper are computed using the closed- form range error expressions explained in the previous section.

For an approaching aircraft, errors in vertical position are most critical. Hence the computed Ionosphere-induced Range Errors (IER) need to be projected onto the vertical direction. The resulting errors are defined as the Ionosphere Induced Error in Vertical (IEV), and the maximum IEV valve is referred to as the Maximum Ionosphere Induced Error in Vertical (MIEV) which is computed as:

$$MIEV_{S_1,S_2} = \left| S_{vert,S_1}\varepsilon_{S_1} + S_{vert,S_2}\varepsilon_{S_2} \right| \quad (4)$$

where:

$S_{vert,i}$: the coefficient of the weighted-least-squares projection matrix $\boldsymbol{S}$ (see [1, 5]) that translates a given amount of range error into vertical position error on satellite *i*.

$(\varepsilon_{S_1}, \varepsilon_{S_2})$: the ionosphere-induced range error values for satellite pair (S_1, S_2).

The largest MIEV value obtained from all possible two-satellite pairs for a particular subset geometry is compared against the tolerable error limit applicable to the current aircraft location from the threshold point. If the MIEV value exceeds the allowable limit, the subset geometry must be made unavailable using the targeted inflation algorithm outlined in subsequent sections.

PROTECTION LEVELS AND THEIR SIGNIFICANCE

GNSS-supported precision approach operations generally have specified Alert Limits (AL) that systems must support. Integrity of the system is compromised when position errors exceed the AL and no alert is issued to the pilot or the flight guidance system within the permitted *time-to-alert*. The LAAS CAT I system is required to meet a time-to-alert of 6 seconds. Based on the aircraft's location within the PAR, vertical alert limits are derived as a function of the Final Approach Segment VAL (FASVAL) and altitude (H_p) as defined in [5]. LAAS CAT I systems support a FASVAL of 10 m.

In order to meet integrity requirements, LAAS provides protection levels that bound residual user errors resulting from error sources such as measurement noise, multipath, nominal ionosphere decorrelation, and ephemeris errors. The vertical protection level (VPL) is defined as the vertical position error value that can be protected with a specified Pr(HMI) (Hazardously Misleading Information) [7]. Three VPL's are computed by the user:

i. Vertical Protection Level under the H_0 hypothesis:

$$VPL_{Apr\ H_0} = K_{ffmd}\sqrt{\sum_{i=1}^{N} s^2_{Apr\ vert,i}\sigma_i^2} \quad (5)$$

where:

K_{ffmd} : multiplier (unitless) which determines the probability of being outside the computed VPL under the H_0 (fault-free) hypothesis. Its value depends on the number of reference receivers used by the LGF.

$s_{Apr\_vert,i}$ ≡ elements of the weighted-least-squares propagation matrix $\boldsymbol{S}$ corresponding to the vertical-axis components for satellite *i*;

σ_i : fault free error variance (in meters) associated with satellite *i*, computed as [5, 6]:

$$\sigma_i^2 = \sigma_{pr\ gnd}^2[i] + \sigma_{tropo}^2[i] + \sigma_{pr\ air}^2[i] + \sigma_{iono}^2[i] \quad (6)$$

where:

$\sigma_{pr\ gnd}[i]$: is the standard deviation of a normal distribution that bounds the SIS contribution to the error in the corrected pseudorange for satellite *i* at the LAAS reference point. At a minimum, it is a function of the satellite elevation angle. In this paper, σ_{pr_gnd} is given by the Ground Accuracy Designator (GAD) C3 LGF error model explained in [5, 6].

$\sigma_{tropo}[i]$: is the standard deviation of a normal distribution associated with the residual tropospheric uncertainty (in meters) for satellite *i* computed by the airborne equipment (see [5]).

$\sigma_{iono}[i]$: is the standard deviation of a normal distribution associated with the residual ionospheric delay uncertainty due to spatial decorrelation for satellite *i* (see [5]).

$\sigma_{pr\ air}[i]$: is the standard deviation of the aircraft contribution to the corrected pseudorange error for satellite *i*. This includes contributions from both the airborne receiver and a standard allowance for airframe multipath. The performance of the airborne subsystem is defined in terms of Airborne Accuracy Designators (AAD). Currently two airborne accuracy designators (A and B) are defined in [5, 6].

Empirical expressions for each of the above sigmas can be obtained from [5, 6].

ii. Vertical Protection Level under the H_1 hypothesis:

As described in [5], a protection-level equation also exists for the H_1 hypothesis, which models a fault in a single LGF reference receiver. The magnitude of VPL_{H1} depends upon the B-values that express discrepancies in the individual pseudorange corrections computed by each LGF reference receiver and which are broadcast to users in real time:

$$VPL_{POS\ H1} = \max\left(VPL_{POS\ H1}[j]\right)$$
$$VPL_{POS\ H1}[j] = \left|B_{j\ POS\ vert}\right| + K_{md\ POS\ vert} \times \sigma_{POS\ vert\ H1} \quad (7)$$

VPL_{H1} is not used in ionosphere-mitigation inflation algorithms for two reasons. The first reason is that, as described below, inflation factors must generally be

computed at least several minutes ahead of time, well before the real-time B-values for a particular epoch will be available. The second reason is that, except for the rare instances when reference receiver failures are present, B-values are driven by nominal error differences among the reference receivers and are small enough that VPL_{H1} stays below VPL_{H0}; thus it very rarely affects the overall VPL (which is the maximum of the three VPL's computed by the user).

iii. Vertical Ephemeris Error Protection Level

An approaching aircraft is required to compute vertical ephemeris error protection levels (VPL_e) if ephemeris error missed detection parameters are broadcast by the LGF. VPL_e values are computed for each satellite in a given geometry subset using the expression:

$$VPL_{Apr\ e}[i] = \left|S_{Apr\ vert,i}\right| x_{air} P[i] + \frac{K_{mde}}{K_{ffmd}} VPL_{Apr\ H_0} \qquad (8)$$

where:

$S_{Apr\_vert,i}$ ≡ elements of the weighted-least-squares propagation matrix $\boldsymbol{S}$ corresponding to the vertical-axis components for satellite i;

x_{air} : Separation between the LGF and the current user aircraft location;

K_{mde} : A broadcast multiplier derived from the probability of missed detection given that there is an ephemeris error on a GPS satellite;

$P[i]$: Ephemeris Decorrelation Parameter broadcast for satellite i. This parameter gives users information regarding the Minimum Ephemeris Detectable Error (MEDE) that can be achieved by the ephemeris monitor. MEDE is the minimum satellite position error that can be detected by the monitor with a probability of missed detection consistent with the integrity risk allocated to ranging source (satellite) failures. Further details about the P-value and its significance can be found in [8].

TARGETED EPHEMERIS DECORRELATION PARAMETER INFLATION ALGORITHM

The concept of determining inflation factors for the broadcast sigmas was originally proposed in [1]. It was proposed that both broadcast sigmas (σ_{vig} and σ_{pr_gnd}) or only σ_{vig} would be inflated using a search algorithm to prevent an approaching aircraft from using potentially unsafe subset geometries. While inflation of σ_{vig} as proposed in [1] eliminated all potentially unsafe subsets, this approach resulted in lower system availability under the updated threat model since only a single σ_{vig} value is broadcast in Message Type 2 of the VDB. However, P-values and σ_{pr_gnd} values are broadcast for each individual ranging source in Message Type 1. The different LAAS VDB message types proposed to be broadcast are defined in [14].

Computing MIEV from range-domain error is proportional to the vertical components of the weighted-least-squares-propagation matrix $\boldsymbol{S}$. The targeted inflation algorithm selects individual ranging sources to be inflated based on their corresponding $S_{Apr\_vert,i}$ values. The ratio of the $S_{Apr\_vert,i}$ value for a satellite in a given unsafe subset to the corresponding value in the all-approved geometry of N satellites helps eliminate the worst satellite without a significant loss in availability.

Targeted P-value inflation works best as the separation between the aircraft and the LGF (x_{air}) increases, as defined in (7). In contrast, σ_{pr_gnd} inflation works well at smaller separations while compromising availability at further separations since the pre-inflated σ_{pr_gnd} is mostly dependent on the elevation of the ranging source. Hence a combination of targeted σ_{pr_gnd} and P-value inflation can result in improved system availability when both close-in and far-away users must be supported. Since LAAS must be able to support multiple runways and approaches at an airport, the LAAS SIS must be able to limit the resultant errors for all of the runway configurations. Hence, a search needs to be performed over a range of separations between the LGF and the threshold point to cover each CAT I approach path at an airport.

Computing σ_{pr_gnd} inflation values for a LGF-to-threshold point separation of 2 km is generally sufficient to eliminate unsafe subsets for 2-km and all shorter LGF-to-threshold separations. This "σ_{pr_gnd} only" initial inflation step covers the majority of approach threshold locations. The satellite-specific σ_{pr_gnd} inflation factors determined are used as an input for the P-value inflation to cover larger LGF-to-threshold separations. The steps in the P-value inflation algorithm are:

Step 1: Inflate P-values for all approved satellites above the nominal level needed to protect users against worst-case ephemeris failures (P_{nom}) [8] until all unsafe subsets become unavailable or until P_A is reached.

Step 2: If unsafe subsets remain, inflate P-values for the satellite with the largest value of the ratio ($S_{vert,\ current\ subset}$) / ($S_{vert,\ all\ in\_view}$) until all unsafe subsets become unavailable or until P_B is reached. If P_B is reached first, repeat inflation from P_A to P_B for the satellite with the second largest value of the above ratio, and repeat as needed until all unsafe subsets are removed or until all satellites have been inflated to P_B.

Step 3: If unsafe subsets remain, inflate P-values for all approved satellites above P_B as much as is needed until all unsafe subsets become unavailable.

Figure 7 graphically illustrates the three steps stated above.

An identical procedure is followed to determine the σ_{pr_gnd} inflation factors for each satellite to protect separations at and below 2 km between the LGF and threshold point. Since the algorithm must run in a run-time environment,

computation time must be kept as low as possible. To accomplish this, a bisection-search algorithm (rather than a simpler linear upward search algorithm) is used to determine the inflation factor for each satellite.

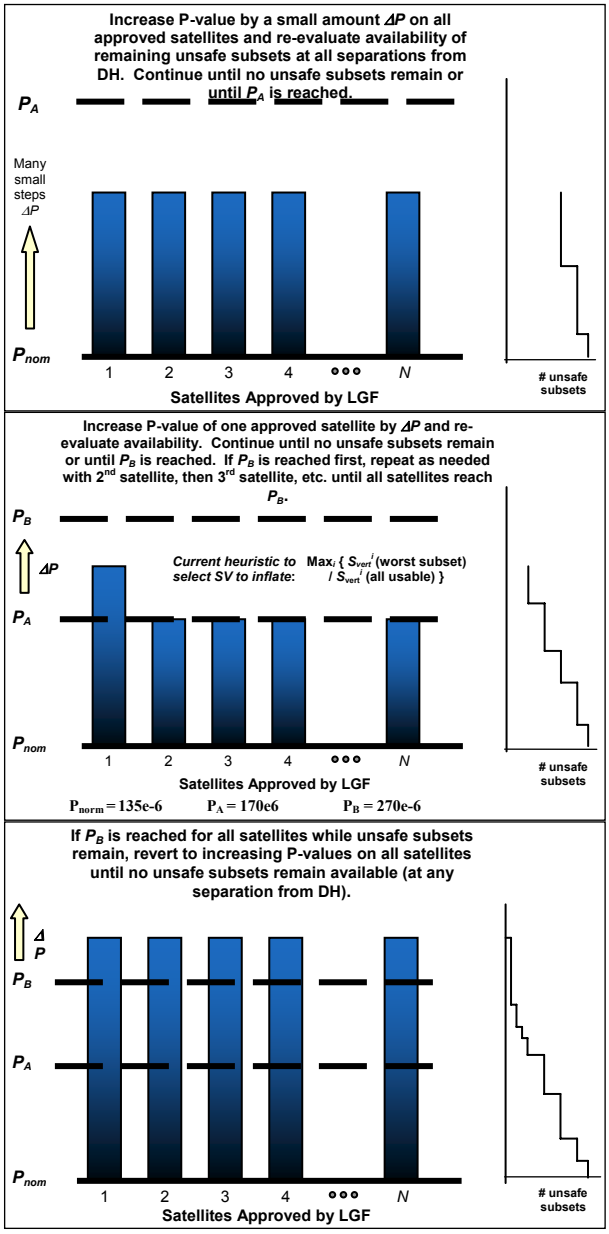

Figure 7: Three Steps in Determining the Targeted P-value and σ_{pr_gnd} Inflation Factors

At this point, it is helpful to clarify the definition of an "unsafe" subset geometry. Keep in mind that a LAAS user aircraft is aware of its current VPL (the maximum of the three VPLs discussed earlier) and the VAL that applies to its current location relative to the threshold of the precision approach it is conducting. In addition, the LGF is also aware of the tolerable error limit the system can support as a function of the distance from the threshold point [12]. An unsafe subset geometry (which could include the "all-approved" geometry) is one whose MIEV exceeds the tolerable error limit for some precision-approach location supported by the LGF while, at the same time, the airborne VPL at that location as predicted by the LGF is below VAL at that location.

As an example, consider a precision approach procedure at a typical airport that ends (i.e., has an approach threshold for a 200-foot DH at) 3 km from the LGF reference point. The tolerable error limit at all threshold locations is 28 meters, while the VAL at all such locations is equal to FASVAL, which is 10 meters for CAT I approaches. If a given satellite geometry that an airborne user might apply has an MIEV exceeding 28 meters and a predicted VPL below the 10-meter VAL, it is unsafe because the airborne user in question, not knowing what its MIEV is (nor what the actual "tolerable error limit" is), would believe that that geometry is safe to use when it is not. Geometries with VPL greater than VAL for all supported locations are safe regardless of MIEV simply because airborne users will see them as "unavailable" and not attempt to conduct precision approaches.

Note that, since VPL for a given geometry is partially a function of σ_{pr_air} in (6), which is an avionics-specific parameter, it cannot be precisely known by the LGF. Therefore, the LGF, when computing VPL, must use the smallest possible value of σ_{pr_air} (i.e., that given by AAD-B in [5]). Finding the smallest possible VPL that a MOPS-compliant aircraft might compute assures that all MOPS-compliant aircraft are protected by the procedure described in this paper. This is the case because minimizing the predicted VPL at the LGF maximizes the chance that VPL will fall below VAL; thus possibly leading to a given subset geometry becoming "unsafe".

The parameter-inflation search methods described above must be repeated for multiple LGF-to-user separations in order to find a single broadcast set of P-values and σ_{pr_gnd} values that supports all separations needed at a given airport. This single broadcast set is comprised of the maximum of the P-values and σ_{pr_gnd} values required by each separation to be supported. The following "pseudocode" shows how all threshold distances out to 6 km from the LGF and aircraft separations out to 7 km beyond the threshold are supported by the real-time search algorithm:

Begin Execution
Compute Inflated σ_{pr_gnd} to protect DH = 2 km. Input for subsequent DH distances.
For DH = 3:6 km {
  For Distance = [DH, DH+1, DH+2, DH+3, DH+7] {
    Determine Unsafe Subsets
      While Exists (Unsafe Subsets)
        P-value = PvalueInflation(DH,Distance,P-value)
      }
    }
  Broadcast Inflated P-values, σ_{pr_gnd} for N "all-in-view" satellites LGF can track
End Execution

A detailed flowchart of the proposed targeted inflation algorithm is shown in Figure 8.

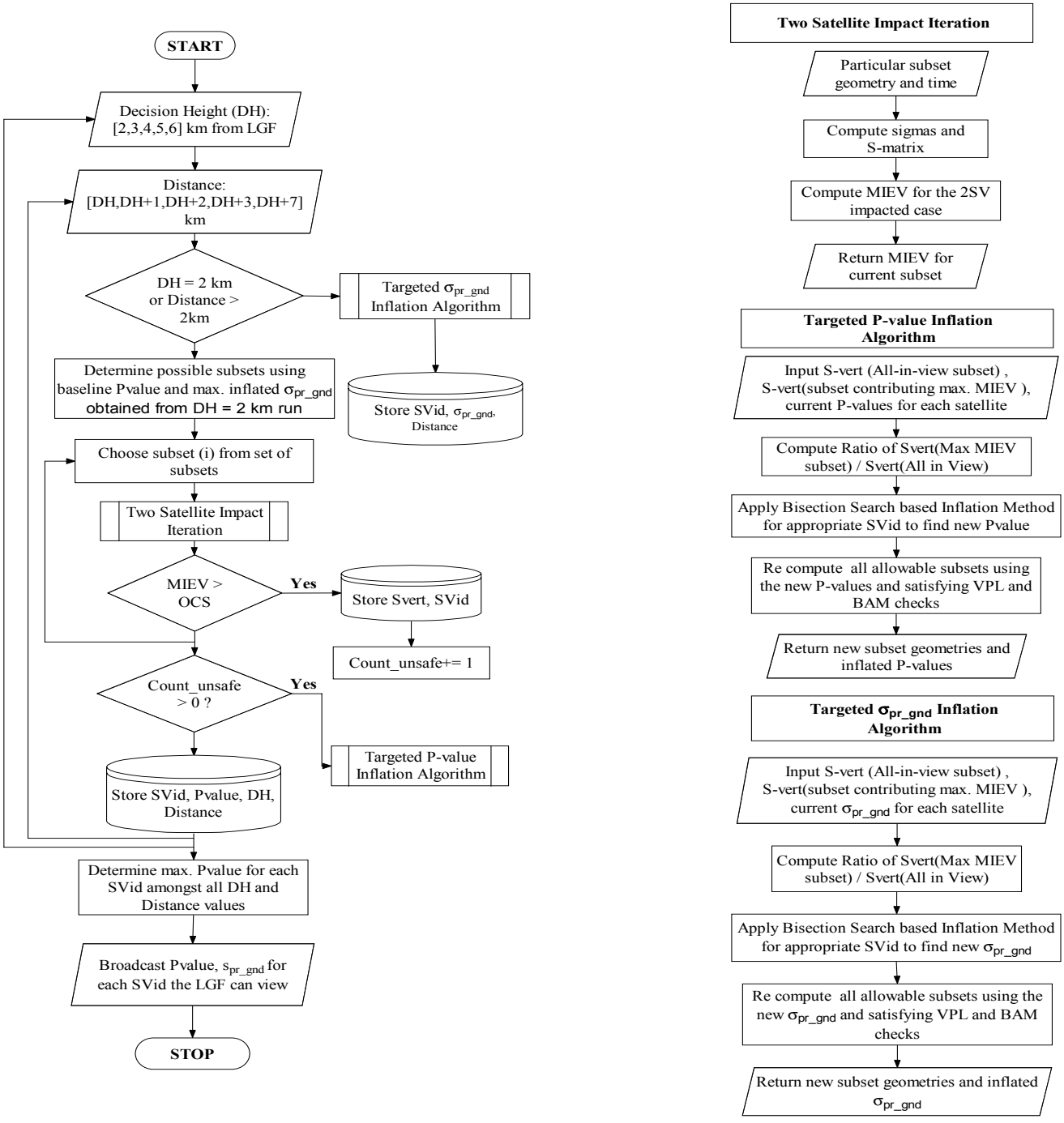

Figure 8: Flow Chart for the Targeted Ephemeris Decorrelation Parameter Inflation Algorithm

SIMULATION AND RESULTS

To evaluate the performance of the proposed algorithm, the standard RTCA 24-satellite GPS constellation as defined in [5] was simulated for 10 major US airports over a 24-hour period of repeating GPS geometries at 5 minute time intervals. Hence there are 288 independent sets of "all-approved" geometries visible to the LGF. Since the allowable error limit is most conservative at the threshold point and anomalous-ionosphere-induced range errors are a function of the separation between the LGF and the aircraft as given by (1), meeting system availability requirements for a threshold point located at 6 km from the LGF (the furthest threshold point planned to be supported by LAAS siting) would be the most demanding. Simulation results for Memphis International Airport (MEM) are discussed in detail. Summary availability results for all 10 U.S. airports simulated are provided to illustrate the improved system availability compared to existing algorithms [2].

Figure 9 shows the vertical and ephemeris protection levels for the all-in-view geometry at MEM for a threshold point located 6 km from the LGF. The "uninflated" protection levels are the values that an aircraft using the "all-approved" satellite geometry would have computed if the broadcast parameters had no anomalous-ionosphere-based inflation. The inflated vertical protection level (VPL_{H0}) is computed using the targeted $\sigma_{pr\ gnd}$ inflation factors determined to protect threshold locations up to 2 km from the LGF. As illustrated in the flowchart and pseudocode, P-value inflation factors are determined for threshold points located at 1-km increments beyond 2 km.

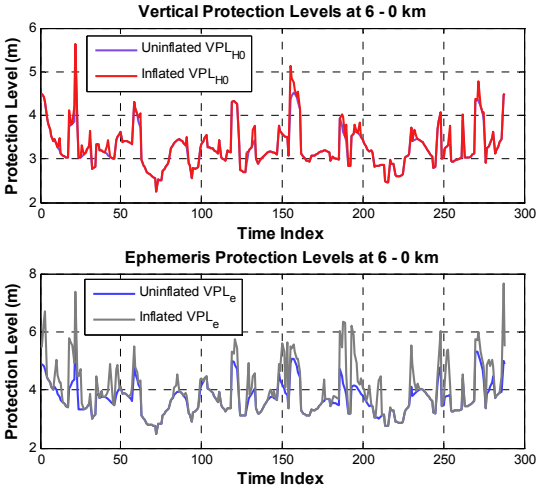

Figure 9: Pre- and Post-Inflation Protection Levels for an Aircraft at a Threshold Point 6 km from the LGF

The VAL curve, which begins at a minimum value of FASVAL (10 meters for CAT I approaches) at the approach threshold, saturates to a constant value of 33.35 meters at a distance of 7 km from the threshold point, as defined in [5]. However, the separately-defined total navigation error limit increases roughly linearly with the distance from the threshold point, as shown in Figure 1 and as derived in [12]. Consequently, for each threshold point, inflation factors must be determined to protect the user from unsafe subsets as far out as 7 km from the threshold. The inflated ephemeris protection levels are determined using the largest P-value obtained during the execution of the iterative loop and the inflated $\sigma_{pr\ gnd}$ values. Availability is maintained for a particular time epoch when the inflated protection levels are below the user alert limits at all supported separations.

Figure 10 represents the resulting MIEVs for a threshold point 6 km from an LGF at MEM. Close to 100 out of the 288 epochs simulated result in MIEVs which exceed the 28-meter total error limit and thereby pose an unacceptable integrity threat. The proposed inflation algorithm eliminates all of these unsafe subsets, resulting in MIEVs at or below the tolerable error limit.

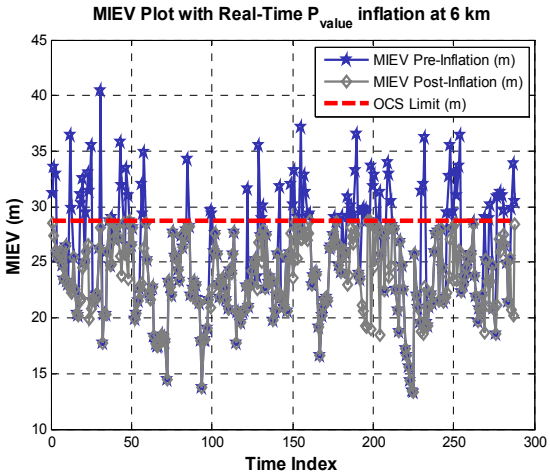

Figure 10: Pre- and Post-Inflation MIEVs for a Threshold Point 6 km from the LGF

Figure 11 illustrates the protection levels for the 6-7 km scenario. The first number in "6-7" stands for the threshold point separation from the LGF, while the second number indicates the additional aircraft separation from the selected threshold. The total separation between the aircraft and the LGF is the sum of these two numbers. P-value inflation causes the ephemeris protection levels to increase. However the maximum inflated protection level is much smaller than the corresponding VAL of 33.35 m.

Figures 9 and 11 illustrate that it is always the inflated protection levels at the threshold location that dictate system availability for this inflation methodology. This is due to the relatively tight (10-meter) VAL applicable at the threshold point.

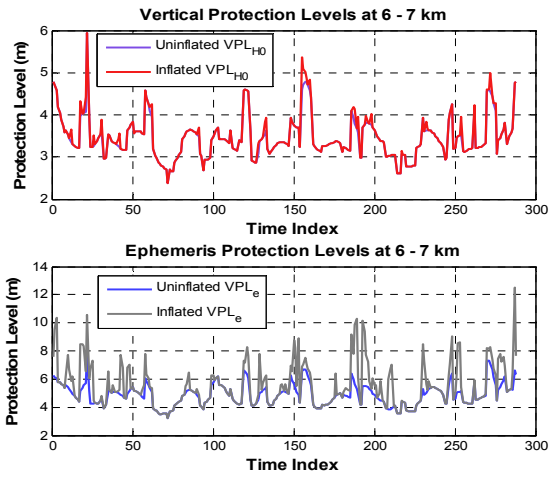

Figure 11: Pre- and Post-Inflation Protection Levels for an Aircraft 7 km Farther Away from a Threshold Point Located 6 km from the LGF

Figure 12 depicts the MIEVs before and after inflation for an aircraft located 13 km from the LGF with the threshold point at 6 km (i.e. the same case as that shown in Figure 8). Since the tolerable error limit linearly increases as the distance from the DH is increased, very few simulation points result in MIEVs which exceed the error limits before inflation. These errors are easily mitigated by the inflated σ_{pr_gnd} and P-values determined to mitigate errors at the threshold locations (since, inflation sufficient to protect the threshold locations is more than adequate to protect longer aircraft separations with larger tolerable error limits).

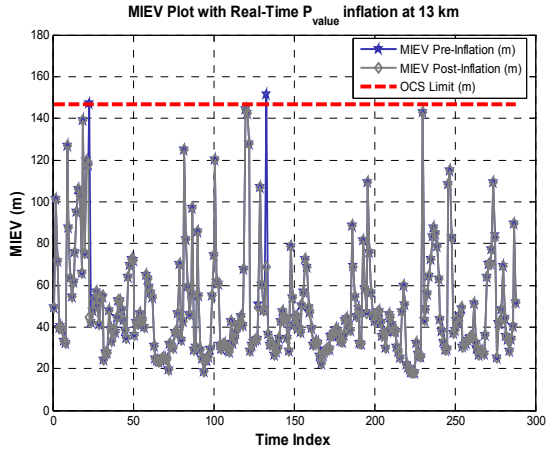

Figure 12: Pre- and Post-Inflation MIEV Plot for an Aircraft located 13 km (6 + 7 km) from the LGF

Figures 13, 14, 15 and 16 are the results obtained for a threshold at MEM located 3 km from the LGF. While Figures 13 and 14 are for the 3-0 scenario, the 3-7 km scenario is analyzed in Figures 15 and 16. Since the worst-case range errors are proportional to the LGF-to-aircraft separation, the resulting vertical position errors are smaller. Thus, fewer simulation points exceed the allowable error limits for the 3-0 km scenario. Also, the inflated protection levels are close to 6 meters providing a margin of 4 meters compared to the 10-meter CAT I VAL at the approach threshold.

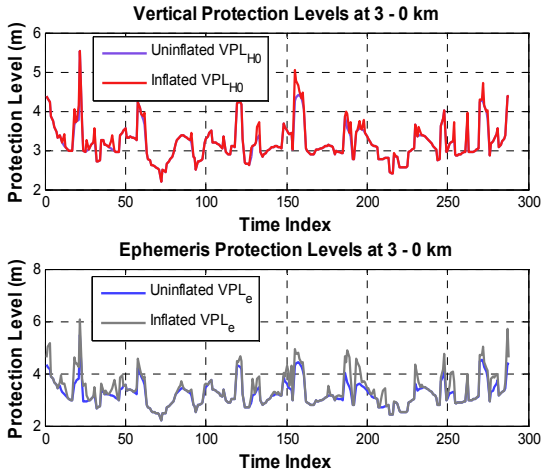

Figure 13: Pre- and Post-Inflation Protection Levels for an Aircraft at a Threshold 3 km from the LGF

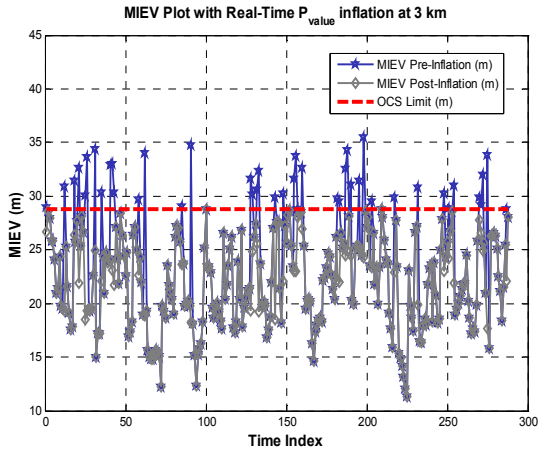

Figure 14: Pre- and Post-Inflation MIEV Plot for an Aircraft Located at a Threshold 3 km from the LGF

Note from Figure 15 that the 3-7 km scenario by itself does not require any inflation since no simulated subset results in an MIEV which exceeds the tolerable error limit. However, since the broadcast inflation factors must protect all airport configurations, which potentially include threshold points as far as 6 km from the LGF, the MIEV values post-inflation will generally still be smaller than the pre-inflation MIEV values since the broadcast inflation factors (driven by more-demanding separations) may eliminate subsets whose MIEV values were marginally smaller than the error limits for this particular scenario. However this does not result in any drop in system availability at MEM.

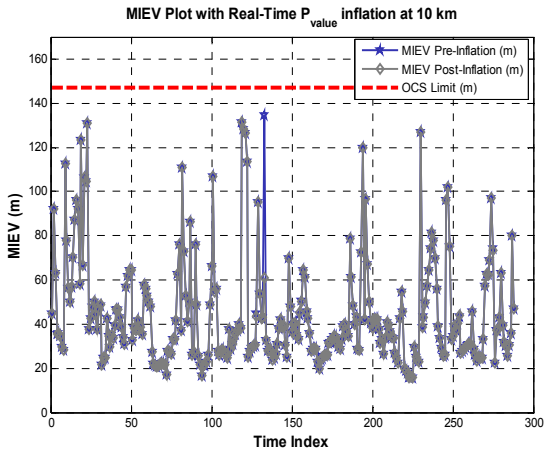

Figure 15: Pre- and Post-Inflation MIEV Plot for an Aircraft Located 10 km (3 + 7 km) from the LGF

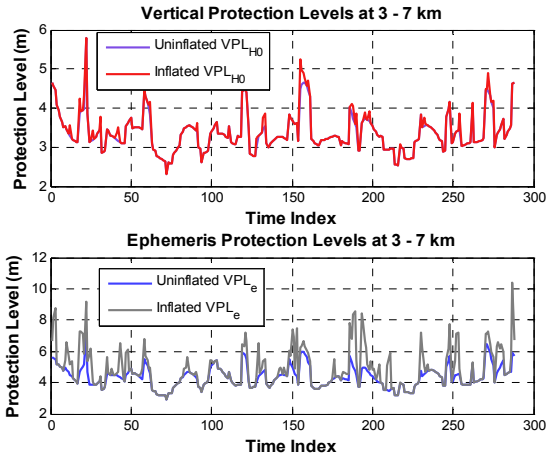

Figure 16: Pre- and Post-Inflation Protection Levels for an Aircraft 10 km (3 + 7 km) from the LGF

Table 1 summarizes the performance of the proposed algorithm for 10 major airports in the Conterminous U.S. The LAAS system should be robust enough to handle any airport where it could potentially be installed. It should also be able to support future airport expansions, such as runway additions. Hence while this table reports results for each airport as though they all require support of approach thresholds as far as 6 km from the LGF, in actual practice, current inflation factors only need to support the CAT I precision approaches that are feasible with the runway and approach configurations that exist when LAAS is fielded. Note from Table 1 that 8 out of the simulated 10 airports result in 100% availability for the worst runway configuration with a threshold/DH situated up to 6 km from the LGF (keep in mind that this result assumes that the aircraft uses the "all-in-view" geometry, which is expected to be the case). Ronald Reagan Washington National Airport (DCA) and the Orlando International Airport (MCO) result in marginally lower system availability. While at MCO, availability drops to 0.99 only for the DH = 6 km case, DCA loses availability for both DH = 5 km and DH = 6 km cases. In reality, DCA itself does not have any runway which could have approach thresholds located more than 4 km from the LGF, and given that DCA is hemmed in on all sides by the Potomac River and other facilities, it is very unlikely to be expanded. Hence the system would have 100% availability under these assumptions for all practical precision approach operations.

It should also be noted that the reason for the drop in availability is due to the poor geometry of the GPS satellites visible at these two airports during the unavailable epochs. In particular, for DCA, the all-in-view geometry itself is unsafe; thus no safe subset geometries are available which aircrafts could potentially use. During such rare periods, sufficient inflation must be applied to make the system unavailable to all CAT I users, including those applying the "all-approved" geometry.

Table 1: Availability for Ten Major U.S. Airports

Airport	RTCA 24 DH=6km	RTCA 24 DH=5 km	RTCA 24 DH=4 km	RTCA 24 DH=3 km	RTCA 24 DH=2 km	RTCA 24 DH=1 km
Memphis (MEM)	1.000	1.000	1.000	1.000	1.000	1.000
Denver (DEN)	1.000	1.000	1.000	1.000	1.000	1.000
Dallas (DFW)	1.000	1.000	1.000	1.000	1.000	1.000
Newark (EWR)	1.000	1.000	1.000	1.000	1.000	1.000
Washington (DCA)	0.993	0.997	1.000	1.000	1.000	1.000
Los Angeles (LAX)	1.000	1.000	1.000	1.000	1.000	1.000
Orlando (MCO)	0.990	1.000	1.000	1.000	1.000	1.000
Minneapolis (MSP)	1.000	1.000	1.000	1.000	1.000	1.000
Chicago (ORD)	0.999	1.000	1.000	1.000	1.000	1.000
Seattle (SEA)	1.000	1.000	1.000	1.000	1.000	1.000

COMPUTATIONAL EFFICIENCY AND REAL-TIME IMPLEMENTATION STRATEGY

The LGF must perform a host of other computations and monitoring apart from ionosphere anomaly monitoring and mitigation. Hence, position-domain geometry screening and parameter-inflation algorithms must be computationally efficient and robust. The computation time for the proposed algorithm to simulate one sample point (one time epoch, giving one all-in-view GPS geometry at a particular location) in Matlab run on an Intel Core 2 Duo 2.2 GHz processor was found to be:

- Average Computation Time: 28.43 seconds per sample point;
- Worst Case Computation Time: 72.12 seconds per sample point.

We believe there is still scope to optimize the current algorithm to further reduce the computation time. The simulations performed for this paper assume a 5-minute time-update interval, and experience with these simulations indicates that a real-time implementation of the algorithm would work fine with the same 5-minute interval if there is no change in the satellite geometry over that interval. Any changes in the satellite geometry that might occur in an upcoming 5-minute interval can be determined by the LGF using the broadcast GPS almanac data. Consequently, the LGF can determine in real time when new satellites will rise and currently-visible satellites will set, allowing it to pre-plan the precise intervals for which inflation simulations need to be run so that each interval maintains a consistent set of "all-approved" satellites.

SUMMARY

Integrity is the most challenging requirement to demonstrate in any precision-approach navigation system. Anomalous ionosphere activities pose a major integrity threat which must be identified and mitigated by the LAAS Ground Facility (LGF). One method of achieving this is through the position-domain geometry screening methodology described in the paper. Such methods are required to render unsafe subsets unavailable to LAAS user aircraft. In this paper, we propose a new satellite-specific or "targeted" inflation algorithm that computes inflation factors on a per-satellite basis for the σ_{pr_gnd} and P-values broadcast via the LAAS VDB Message Type 1. This algorithm was simulated for 10 major U.S. airports, and its performance was evaluated. While being computationally efficient, this algorithm results in both improved availability and flexibility compared to other existing inflation algorithms.

ACKNOWLEDGEMENTS

This work was funded by the affiliated members of the Stanford Center for Position, Navigation, and Time (SCPNT) and the FAA Satellite Navigation LAAS Program Office. Their support is greatly appreciated. However, the opinions expressed within this paper are solely those of the authors.

REFERENCES

1. J. Lee, *et al.*, "Position-Domain Geometry Screening to Maximize LAAS Availability in the Presence of Ionosphere Anomalies," *Proceedings of ION GNSS 2006*, Fort Worth, TX, Sept. 26-29, 2006.
2. Enge, P., *et al.*, "GBAS Ionosphere", *6th International GBAS Working Group Meeting*, Seattle, WA, July 17-20, 2007.
3. A. Ene, *et al.*, "A Comprehensive Ionosphere Storm Data Analysis Method to Support LAAS Threat Model Development," *Proceedings of ION 2005 National Technical Meeting*, San Diego, CA, Jan. 24-26, 2005, pp. 110-130.
4. P. Misra, P. Enge, *Global Positioning System: Signals, Measurements and Performances*. Ganga-Jamuna Press, Lincoln, MA, 2006
5. *Minimum Operational Performance Standards for Local Area Augmentation System (LAAS)*. Washington, DC, RTCA SC-159, WG-4, DO-253B, June 26, 2007.
6. *Minimum Aviation System Performance Standards for Local Area Augmentation System (LAAS)*. Washington, DC, RTCA SC-159, WG-4, DO-245A, December 9, 2004.
7. Enge, P., "Local Area Augmentation of GPS for the Precision Approach of Aircraft", *Proceedings of the IEEE,* Vol. 87, No. 1, January 1999.
8. Pervan, B., L. Gratton "Orbit Ephemeris Monitors for Local Area Differential GPS", *IEEE Transactions on Aerospace and Electrical Systems,* Vol. 41, No. 2, April 2005.
9. M. Luo, *et al.*, "LAAS Study of Slow-Moving Ionosphere Anomalies and their Potential Impacts", *Proceedings of the ION GNSS 2005,* Long Beach, CA, September 13-16, 2005, pp. 2337-2339.
10. S. Datta-Barua, *et al.*, "Using WAAS Ionospheric Data to Estimate LAAS Short Baseline Gradients", *Proceedings of the ION 2002 National Technical Meeting*. Anaheim, CA, January 28-30, 2002, pp. 523-530.
11. Shively, C., Young C. Lee, "A Position-Domain Ground Based Integrity Method for LAAS", *Proceedings of ION GPS 1996*, Kansas City, MO, September 17-20, 1996, pp. 1645-1656.
12. Shively, C., "Safety Concepts for Mitigation of Ionospheric Anomaly Errors in GBAS", *Proceedings of the ION 2008 National Technical Meeting*, San Diego, CA, January 28-30, 2008.
13. *Algorithm Description Document for Ionosphere Anomaly Mitigation within the Local Area Augmentation System Ground Facility*. Stanford University LAAS Laboratory, Stanford, CA, Honeywell International, Coon Rapids, MN, Version 1.0, August 30, 2006.
14. *GNSS-Based Precision Approach Local Area Augmentation System (LAAS) Signal-in-Space Interface Control Document.* Washington, DC, RTCA SC-159, WG-4, DO-246C, April 7, 2005.
15. Lee, J., S. Pullen, S. Datta-Barua, and P. Enge, "Assessment of Ionosphere Spatial Decorrelation for Global Positioning System-Based Aircraft Landing Systems", *AIAA Journal of Aircraft*, Vol. 44, No. 5, Sept.-Oct. 2007, pp. 1662-1669.
16. Simili, D.V., B. Pervan, "Code-Carrier Divergence Monitoring for the GPS Local Area Augmentation System, *Proceedings of IEEE/ION PLANS 2006*, San Diego, CA, April 25-27, 2006, pp. 483-493.